The Astrophysical Journal Letters, 883:L7 (6pp), 2019 September 20 https://doi.org/10.3847/2041-8213/ab40c0

Binary Mergers near a Supermassive Black Hole: Relativistic Effects in Triples

Bin Liu[1], Dong Lai[1,2], and Yi-Han Wang[3]
[1] Cornell Center for Astrophysics and Planetary Science, Cornell University, Ithaca, NY 14853, USA
[2] Tsung-Dao Lee Institute, Shanghai Jiao Tong University, Shanghai 200240, People's Republic of China
[3] Department of Physics and Astronomy, Stony Brook University, Stony Brook, NY 11794-3800, USA
Received 2019 August 4; revised 2019 August 29; accepted 2019 August 31; published 2019 September 18

Abstract

We study the general relativistic (GR) effects induced by a spinning supermassive black hole on the orbital and spin evolution of a merging black hole binary (BHB) in a hierarchical triple system. A sufficiently inclined outer orbit can excite Lidov–Kozai eccentricity oscillations in the BHB and induce its merger. These GR effects generate extra precessions on the BHB orbits and spins, significantly increasing the inclination window for mergers and producing a wide range of spin orientations when the BHB enters LIGO band. This "GR-enhanced" channel may play an important role in BHB mergers.

Unified Astronomy Thesaurus concepts: Astrophysical processes (104); Gravitation (661); Gravitational waves (678); Gravitational wave sources (677)

1. Introduction

The detections of gravitational waves (GWs) from merging binary black holes (BHs; e.g., Abbott et al. 2018a, 2018b; Venumadhav et al. 2019; Zackay et al. 2019) have motivated many recent studies on the dynamical formation of such compact black hole binaries (BHBs). Dynamical formation channels include mergers arising from strong gravitational scattering in dense clusters (e.g., Portegies & McMillan 2000; O'Leary et al. 2006; Miller & Lauburg 2009; Banerjee et al. 2010; Downing et al. 2010; Ziosi et al. 2014; Samsing & Ramirez-Ruiz 2017; Gondán et al. 2018; Rodriguez et al. 2018; Samsing et al. 2018; Samsing & D'Orazio 2018) and more gentle "tertiary-induced mergers"—the latter can take place either in isolated triple/quadrupole systems (e.g., Antonini et al. 2017; Liu & Lai 2017, 2018; Silsbee & Tremaine 2017; Liu et al. 2019) or in nuclear clusters dominated by a central supermassive BH (SMBH; e.g., Antonini & Perets 2012; VanLandingham et al. 2016; Petrovich & Antonini 2017; Hamers et al. 2018; Hoang et al. 2018; Randall & Xianyu 2018; Frangione et al. 2019).

In this Letter we are interested in stellar-mass BHB mergers induced by an SMBH. Such BHBs may exist in abundance in the nuclear cluster around the SMBH due to various dynamical processes, such as scatterings and mass segregation (e.g., O'Leary et al. 2009; Leigh et al. 2018). Gravitational perturbation from the SMBH induces Lidov–Kozai (LK) eccentricity oscillations of the BHB, which leads to enhanced gravitational radiation and merger of the BHB. Our Letter examines several general relativistic (GR) effects that were overlooked in previous studies, but significantly impact the efficiency and outcomes of LK-induced mergers. We focus on isolated BHB–SMBH systems, and do not consider other processes related to scatterings and relaxation with surrounding stars in the cluster (e.g., VanLandingham et al. 2016; Petrovich & Antonini 2017; Hamers et al. 2018), which may also change the character of LK-induced mergers.

In the *Standard LK-Induced Merger* scenario, a BHB with masses m_1, m_2, semimajor axis $a_{\rm in}$, and eccentricity $e_{\rm in}$, moves around a tertiary (m_3) on a wider orbit with $a_{\rm out}$ and $e_{\rm out}$. The angular momenta of the inner and outer binaries are denoted by $\boldsymbol{L}_{\rm in} \equiv {\rm L}_{\rm in}\hat{\boldsymbol{L}}_{\rm in}$ and $\boldsymbol{L}_{\rm out} \equiv {\rm L}_{\rm out}\hat{\boldsymbol{L}}_{\rm out}$ (where $\hat{\boldsymbol{L}}_{\rm in}$ and $\hat{\boldsymbol{L}}_{\rm out}$ are unit vectors). If the mutual inclination between $\hat{\boldsymbol{L}}_{\rm in}$ and $\hat{\boldsymbol{L}}_{\rm out}$ (denoted as I) is sufficiently high, the inner binary would experience LK eccentricity oscillations on the timescale

$$t_{\rm LK} = \frac{1}{\Omega_{\rm LK}} = \frac{1}{n_{\rm in}}\frac{m_{12}}{m_3}\left(\frac{a_{\rm out,eff}}{a_{\rm in}}\right)^3, \quad (1)$$

where $m_{12} \equiv m_1 + m_2$, $n_{\rm in} = (Gm_{12}/a_{\rm in}^3)^{1/2}$ is the mean motion of the inner binary, and $a_{\rm out,eff} \equiv a_{\rm out}\sqrt{1-e_{\rm out}^2}$ is the effective outer binary separation.

GR introduces pericenter precession of the inner binary, which can be described by the first-order post-Newtonian (PN) theory

$$\left.\frac{d\boldsymbol{e}_{\rm in}}{dt}\right|_{\rm GR} = \dot{\omega}_{\rm GR}\hat{\boldsymbol{L}}_{\rm in}\times\boldsymbol{e}_{\rm in},\ \dot{\omega}_{\rm GR} = \frac{3Gn_{\rm in}m_{12}}{c^2a_{\rm in}(1-e_{\rm in}^2)}. \quad (2)$$

This precession competes with $\Omega_{\rm LK}$, and tends to suppress LK oscillations or limit the maximum eccentricity $e_{\rm max}$ (e.g., Fabrycky & Tremaine 2007; Liu et al. 2015). The general secular and quasi-secular equations of motion (see vector form in Liu et al. 2015; Liu & Lai 2018; Petrovich 2015), combined with the GW radiation, completely determine the evolution of the triple system. Such LK-induced mergers have been extensively studied (e.g., Blaes et al. 2002; Miller & Hamilton 2002; Wen 2003; Antonini & Perets 2012; Liu & Lai 2017, 2018; Silsbee & Tremaine 2017; Liu et al. 2019).

The spin vector ($\boldsymbol{S}_1 \equiv {\rm S}_1\hat{\boldsymbol{S}}_1$) of the BH is also coupled to the orbital angular momentum vector $\boldsymbol{L}_{\rm in}$ through de-Sitter precession (1.5 PN effect; e.g., Barker & O'Connell 1975):

$$\left.\frac{d\hat{\boldsymbol{S}}_1}{dt}\right|_{{\rm S_1L_{in}}} = \Omega_{\rm S_1L_{in}}\hat{\boldsymbol{L}}_{\rm in}\times\hat{\boldsymbol{S}}_1,\quad \Omega_{\rm S_1L_{in}} = \frac{3Gn_{\rm in}(m_2+\mu_{\rm in}/3)}{2c^2a_{\rm in}(1-e_{\rm in}^2)}, \quad (3)$$

where $\mu_{\rm in} \equiv m_1m_2/m_{12}$ is the reduced mass for the inner binary. A similar equation applies to the spinning body 2. To determine the final spin–orbit misalignments of the BHBs, it is essential to include this spin–orbit coupling effect in the scenario of the LK-induced merger. Our recent works (e.g., Liu

& Lai 2017, 2018; Liu et al. 2019), focusing on the BHB mergers induced by stellar-mass tertiary (m_3 comparable to m_1, m_2), have shown that LK-induced mergers can give rise to unique signatures for the final spin–orbit misalignment angle $\theta_{\rm sl}^{\rm f}$ (see also Antonini et al. 2018; Rodriguez & Antonini 2018). In particular, for initially close BHBs (with $a_0 \lesssim 0.2$ au), which can merge without the aid of the tertiary companion, modest ($\lesssim 40°$) $\theta_{\rm sl}^{\rm f}$ can be produced in the majority of triples (e.g., Liu & Lai 2017). For wide binaries (with $a_0 \gtrsim 10$ au), the distribution of $\theta_{\rm sl}^{\rm f}$ is peaked around 90° if the BHs have comparable masses (negligible octupole effect), while a more isotropic distribution of final spin axis is produced as the octupole effect increases (e.g., Liu & Lai 2018; Liu et al. 2019).

The *Standard LK-Induced Merger* mechanism, as outlined above (and studied in all previous works), includes the key GR effects associated with the inner binaries, but neglects the GR effects associated with the tertiary companion. This is adequate when the tertiary mass m_3 is not much larger than the masses of the inner BHB. However, for BHB–SMBH triples, with $m_3 \gg m_1$, m_2, several GR effects involving the SMBH can qualitatively change the efficiency and outcomes of LK-induced mergers.

2. New GR Effects Involving SMBH Tertiary

We start by examining how various GR effects associated with the SMBH tertiary affect the LK oscillations and spin evolution of the inner BHB (see Figure 1).

(i) *Effect I: Lense–Thirring Precession of* $\boldsymbol{L}_{\rm out}$ *around* $\boldsymbol{S}_3$. For an SMBH, the spin angular momentum $S_3 = \chi_3 G m_3^2/c$ (where $\chi_3 \leqslant 1$ is the Kerr parameter) can be easily larger than $L_{\rm out} = \mu_{\rm out}\sqrt{G m_{\rm tot} a_{\rm out}(1-e_{\rm out}^2)}$ (where $\mu_{\rm out} \equiv (m_{12}m_3)/m_{\rm tot}$ and $m_{\rm tot} = m_{12} + m_3$). Thus $\boldsymbol{L}_{\rm out}$ experiences Lense–Thirring precession around $\boldsymbol{S}_3$ if the two vectors are misaligned (1.5 PN effect; e.g., Barker & O'Connell 1975; Fang & Huang 2019):

$$\left.\frac{d\boldsymbol{L}_{\rm out}}{dt}\right|_{\rm L_{out}S_3} = \Omega_{\rm L_{out}S_3}\hat{\boldsymbol{S}}_3 \times \boldsymbol{L}_{\rm out},$$

$$\left.\frac{d\boldsymbol{e}_{\rm out}}{dt}\right|_{\rm L_{out}S_3} = \Omega_{\rm L_{out}S_3}\hat{\boldsymbol{S}}_3 \times \boldsymbol{e}_{\rm out} \quad (4)$$

$$-3\Omega_{\rm L_{out}S_3}(\hat{\boldsymbol{L}}_{\rm out}\cdot\hat{\boldsymbol{S}}_3)\hat{\boldsymbol{L}}_{\rm out}\times\boldsymbol{e}_{\rm out}, \quad (5)$$

where the orbit-averaged precession rate is

$$\Omega_{\rm L_{out}S_3} = \frac{G S_3(4+3m_{12}/m_3)}{2c^2 a_{\rm out}^3(1-e_{\rm out}^2)^{3/2}}. \quad (6)$$

The back-reaction of Equation (4) implies that $\boldsymbol{S}_3$ precesses around $\boldsymbol{L}_{\rm out}$ at the rate $\Omega_{\rm L_{out}S_3}L_{\rm out}/S_3$.

As shown in Hamers & Lai (2017) in a different context, the variation of $\hat{\boldsymbol{L}}_{\rm out}$ can significantly affect LK eccentricity excitation when $\Omega_{\rm L_{out}S_3}$ becomes comparable to $\Omega_{\rm LK}$. As shown in Figure 1, $\Omega_{\rm L_{out}S_3}/\Omega_{\rm LK} \sim 1$ can be satisfied for sufficiently large m_3 ($\gtrsim 10^9 M_\odot$). More precisely, LK oscillations can be affected or triggered due to an inclination resonance, which occurs when $\Omega_{\rm L_{out}S_3}$ matches $\Omega_{\rm L_{in}L_{out}}$, the precession rate of $\hat{\boldsymbol{L}}_{\rm in}$ around $\hat{\boldsymbol{L}}_{\rm out}$ (see below).

Figure 2 depicts an example of how various relativistic effects associated with the SMBH modify LK oscillations. The results are obtained by integrating the double-averaged (DA) secular equations of motion (averaging over both the inner and outer orbits; e.g., Liu et al. 2015; Liu & Lai 2018). We see that

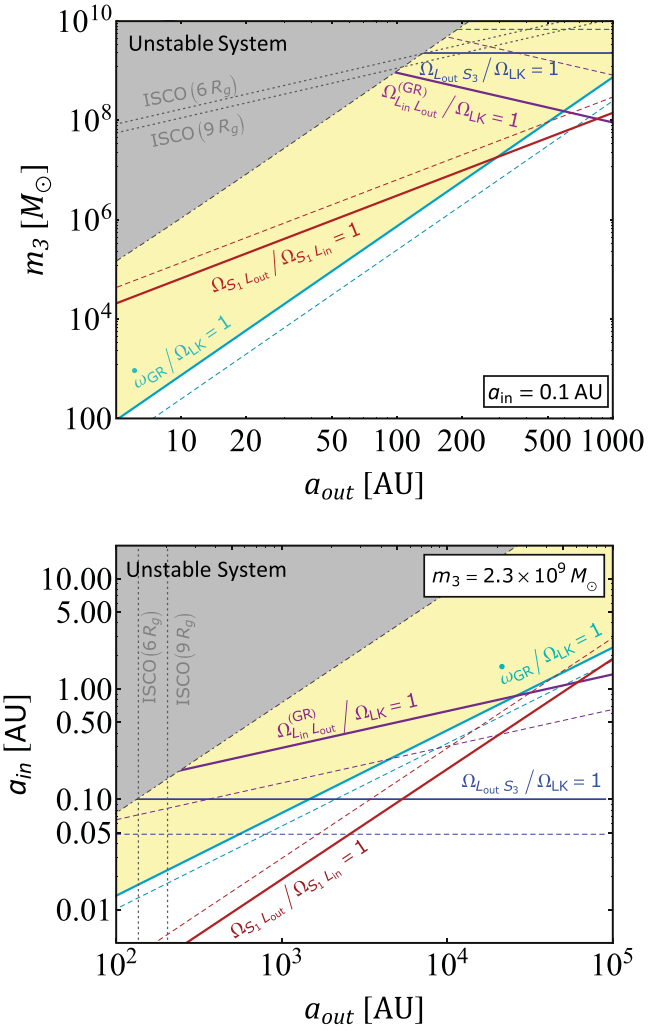

Figure 1. Parameter space in the m_3–$a_{\rm out}$ plane and $a_{\rm in}$–$a_{\rm out}$ plane indicating the relative importance of various GR effects. The yellow region corresponds to the space where LK oscillations in the BHB are not suppressed by GR-induced apsidal precession ($\dot{\omega}_{\rm GR}/\Omega_{\rm LK} < 1$) and the triple system is dynamically stable (the dotted–dashed line is the instability limit according to Kiseleva et al. 1996). All the solid lines are evaluated when the ratio of relevant frequencies is equal to unity (as labeled) and the dashed lines indicate that the ratio is equal to 3. The dotted lines indicate the innermost stable circular orbits (ISCO) for the outer binary, where $R_g = (Gm_3)/c^2$ (the ISCO ranges from R_g to $9R_g$ depending on the spin magnitude and orientation relative to the orbit). The other parameters are $m_1 = 30M_\odot$, $m_2 = 20M_\odot$, $e_{\rm in} = e_{\rm out} = 0$, and $\chi_3 = 1$.

the BHB eccentricity exhibits regular oscillations in the "standard LK" case (black lines), but the inclusion of Effect I (Equations (4)–5) (purple lines) makes the eccentricity evolve chaotically and extend to higher values.

(ii) *Effect II: de-Sitter-like Precession of* $\boldsymbol{L}_{\rm in}$ *around* $\boldsymbol{L}_{\rm out}$. The standard LK mechanism already includes the Newtonian precession of $\boldsymbol{L}_{\rm in}$ around $\boldsymbol{L}_{\rm out}$ (driven by the tidal potential of m_3 on the inner orbit), at the rate given by (to quadrupole order)[4]

$$\Omega^{\rm (N)}_{\rm L_{in}L_{out}} = -\frac{3}{4}\Omega_{\rm LK}(\hat{\boldsymbol{L}}_{\rm out}\cdot\hat{\boldsymbol{L}}_{\rm in}) \qquad (\text{for } e_{\rm in}=0). \quad (7)$$

[4] The general equation for finite $e_{\rm in}$ can be found in Liu et al. (2015). Note that for BHB–SMBH systems ($m_3 \gg m_{12}$), dynamical stability requires $a_{\rm out} \gg a_{\rm in}$. Thus, the octupole LK is negligible since $\varepsilon_{\rm oct} \equiv [(m_1-m_2)/(m_1+m_2)](a_{\rm in}/a_{\rm out})[e_{\rm out}/(1-e_{\rm out}^2)] \ll 1$.

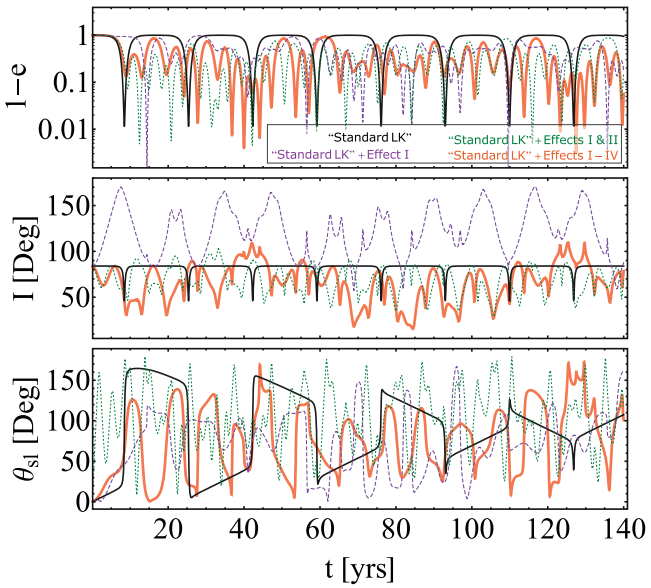

Figure 2. Sample orbital and spin evolution of a BHB with an SMBH tertiary. The three panels show the eccentricity, the inclination of the inner BH binary (the angle between $\hat{\boldsymbol{L}}_{\rm in}$ and $\hat{\boldsymbol{L}}_{\rm out}$), and the spin–orbit misalignment (the angle between $\hat{\boldsymbol{S}}_1$ and $\hat{\boldsymbol{L}}_{\rm in}$). The parameters are $m_1 = 30M_\odot$, $m_2 = 20M_\odot$, $a_{\rm in} = 0.1$ au, $m_3 = 2.3 \times 10^9 M_\odot$, $a_{\rm out} = 500$ au, $e_{\rm out} = 0$, and the initial $e_{\rm in,0} = 0.001$, $I_0 = 84°$ and $\theta_{\rm sl}^0 = 0°$. The color-coded trajectories represent the evolution with various effects included (as labeled). Gravitational radiation is not included in these examples.

In GR, $\boldsymbol{L}_{\rm in}$ experiences an additional de-Sitter-like (geodesic) precession in the gravitational field of m_3, such that the net precession of $\boldsymbol{L}_{\rm in}$ around $\boldsymbol{L}_{\rm out}$ is governed by

$$\left.\frac{d\boldsymbol{L}_{\rm in}}{dt}\right|_{\rm L_{in}L_{out}} = \Omega_{\rm L_{in}L_{out}} \hat{\boldsymbol{L}}_{\rm out} \times \boldsymbol{L}_{\rm in}, \tag{8}$$

with $\Omega_{\rm L_{in}L_{out}} \equiv \Omega^{\rm (N)}_{\rm L_{in}L_{out}} + \Omega^{\rm (GR)}_{\rm L_{in}L_{out}}$, and

$$\Omega^{\rm (GR)}_{\rm L_{in}L_{out}} = \frac{3}{2}\frac{G(m_3 + \mu_{\rm out}/3)n_{\rm out}}{c^2 a_{\rm out}(1-e_{\rm out}^2)}, \tag{9}$$

where $n_{\rm out} = (Gm_{\rm tot}/a_{\rm out}^3)^{1/2}$. To keep $\boldsymbol{L}_{\rm in} \cdot \boldsymbol{e}_{\rm in} = 0$, we also need to add $d\boldsymbol{e}_{\rm in}/dt = \Omega^{\rm (GR)}_{\rm L_{in}L_{out}} \hat{\boldsymbol{L}}_{\rm out} \times \boldsymbol{e}_{\rm in}$ to the eccentricity evolution equation. We can safely neglect the feedback from $\hat{\boldsymbol{L}}_{\rm in}$, $\boldsymbol{e}_{\rm in}$ on $\hat{\boldsymbol{L}}_{\rm out}$ and $\boldsymbol{e}_{\rm out}$. Equation (9) has the same form as Equation (3), but can also be reproduced through the "cross terms" in the PN equations of motion of hierarchical triple systems (C. Will 2019, private communication; see also Will 2014, 2018).

Note that for the standard LK mechanism (and with negligible octupole effect, as valid for the $m_3 \gg m_{12}$ case considered in this Letter), the nodal precession of $\boldsymbol{L}_{\rm in}$ around $\boldsymbol{L}_{\rm out}$ is decoupled from the LK eccentricity/inclination oscillations. Therefore adding $\Omega^{\rm (GR)}_{\rm L_{in}L_{out}}$ (Effect II) to $\Omega_{\rm L_{in}L_{out}}$ by itself does not alter the $e_{\rm in}$-excitation (although it can affect the spin evolution). However, when combined with Effect I, it can significantly affect LK oscillation (see Figure 2, dotted green line). We quantify this behavior by defining the dimensionless ratio

$$\gamma \equiv \frac{\Omega_{\rm L_{in}L_{out}}}{\Omega_{\rm L_{out}S_3}} = \frac{\Omega^{\rm (N)}_{\rm L_{in}L_{out}} + \Omega^{\rm (GR)}_{\rm L_{in}L_{out}}}{\Omega_{\rm L_{out}S_3}}. \tag{10}$$

Since $\Omega^{\rm (N)}_{\rm L_{in}L_{out}}$ depends on I [where $\hat{\boldsymbol{L}}_{\rm out} \cdot \hat{\boldsymbol{L}}_{\rm in} = \cos I$], γ ranges from $\gamma_{\rm min} = \gamma\ (I = 0°)$ to $\gamma_{\rm max} = \gamma\ (I = 180°)$.

As explained in Hamers & Lai (2017), when $\gamma \sim 1$, an inclination resonance generates larger I even from a small initial I_0, leading to a wider range of initial inclinations for extreme eccentricity excitation. Figure 3 explores these new GR effects by showing the $e_{\rm in}$-excitation window as a function of I_0 for BHB–SMBH systems with given m_1, m_2, $a_{\rm in}$, $a_{\rm out}$ but different values of m_3 (thus different γ's). The misalignment angle between $\hat{\boldsymbol{S}}_3$ and $\hat{\boldsymbol{L}}_{\rm out}$ is set to 30°, but with a random azimuthal phase angle (i.e., the initial $\hat{\boldsymbol{L}}_{\rm in}$, $\hat{\boldsymbol{L}}_{\rm out}$, and $\hat{\boldsymbol{S}}_3$ are not in the same plane[5]). By evolving the triple system using the DA secular equations, we record $e_{\rm max}$ achieved over an integration timespan of 500 $t_{\rm LK}$ for each system with and without Effects I, II, and IV. In each panel, the cyan dots are the "standard LK" results; these can be calculated analytically (e.g., Liu et al. 2015). Note that since the octupole-order effects are negligible, systems with finite $e_{\rm out}$ should exhibit a similar behavior as the cyan dots. We see that including Effects I–II (purple dots) can dramatically widen the eccentricity excitation window. As γ approaches unity with increasing m_3, overlapping inclination and LK resonances give rise to the widespread chaos (e.g., Hamers & Lai 2017), causing systems with modest I_0 to attain extreme eccentricity growth.

When $e_{\rm max}$ becomes sufficiently close to unity, the timescale the inner BHB spends in high-$e_{\rm in}$ phase ($t_{\rm LK}\sqrt{1-e_{\rm max}^2}$; e.g., Anderson et al. 2016) becomes less than the period of the outer binary, the DA approximation breaks down, and the system enters the semisecular regime (e.g., Luo et al. 2016). If it is shorter than the inner orbital period, the evolution of triples can only be resolved correctly by N-body integration. In Figure 3, the systems in the bottom right panel belong to the semisecular regime. To better address the orbital evolution, we also integrate the single-averaged (SA) secular equations (only averaging over the inner orbital period; e.g., Liu & Lai 2018). The result (light blue dots) shows that the eccentricity in SA integrations can undergo excursions to even more extreme values.

(iii) *Effect III*: de-Sitter Precession of $\boldsymbol{S}_1$ around $\boldsymbol{L}_{\rm out}$. The "standard LK" already includes de-Sitter precession of $\boldsymbol{S}_1$ around $\boldsymbol{L}_{\rm in}$. With an SMBH tertiary, $\boldsymbol{S}_1$ also experiences a precessional torque from m_3:

$$\left.\frac{d\hat{\boldsymbol{S}}_1}{dt}\right|_{\rm S_1L_{out}} = \Omega_{\rm S_1L_{out}} \hat{\boldsymbol{L}}_{\rm out} \times \hat{\boldsymbol{S}}_1, \tag{11}$$

with

$$\Omega_{\rm S_1L_{out}} = \frac{3}{2}\frac{G(m_3 + \mu_{\rm out}/3)n_{\rm out}}{c^2 a_{\rm out}(1-e_{\rm out}^2)}. \tag{12}$$

Note that $\Omega_{\rm S_1L_{out}} = \Omega^{\rm (GR)}_{\rm L_{in}L_{out}}$ (Equation (9)). The back-reaction torques on $\hat{\boldsymbol{L}}_{\rm out}$ and $\hat{\boldsymbol{e}}_{\rm out}$ can be safely neglected since $\rm L_{out} \gg S_1$. Although Equation (11) does not affect the orbital evolution of the inner binary, it does affect the evolution of $\boldsymbol{S}_1$ and the spin–orbit misalignment angle $\theta_{\rm sl}$.

The bottom panel of Figure 2 shows several examples of the evolution of $\theta_{\rm sl}$ during LK oscillations, with and without various GR effects. The evolution of $\boldsymbol{S}_1$ is governed by two

[5] Note that in examples shown in Hamers (2018) and Liu & Lai (2019), the phase angle is set to be fixed, where $\hat{\boldsymbol{L}}_1$, $\hat{\boldsymbol{L}}_2$, and $\hat{\boldsymbol{L}}_{\rm out}$ initially lie in the same plane.

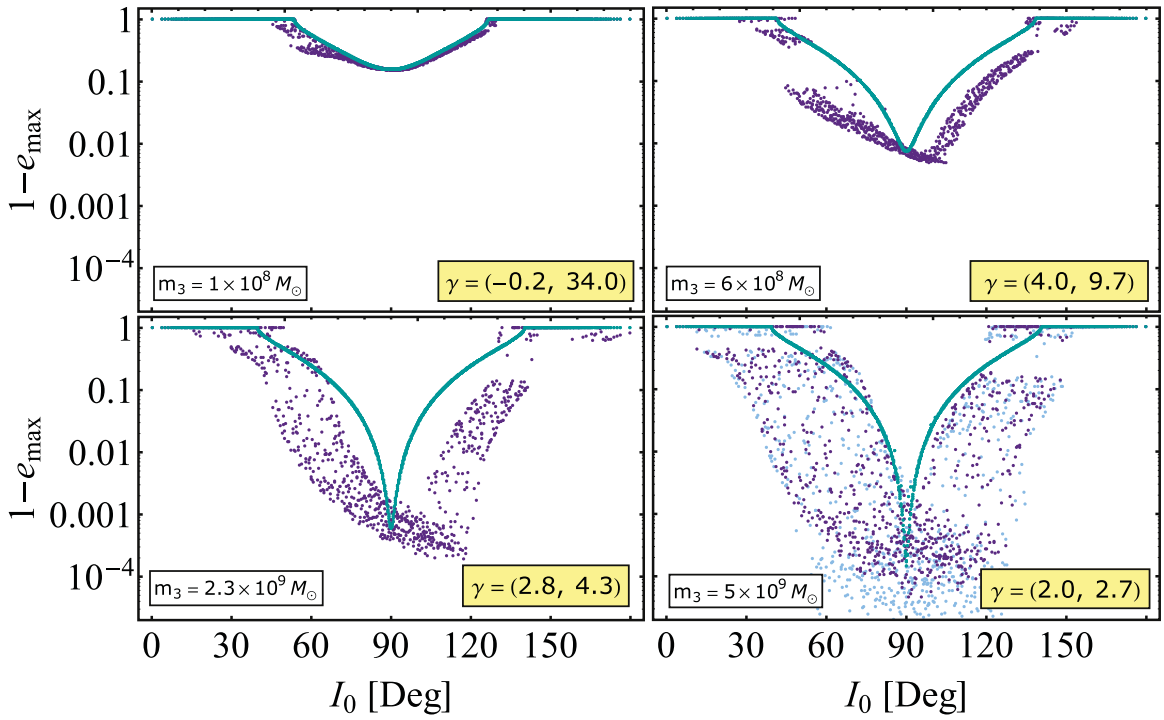

Figure 3. Maximum eccentricity of the inner BHB vs. the initial inclination I_0 for different SMBH masses (as labeled). The inner binary has $m_1 = 30M_\odot$, $m_2 = 20M_\odot$, and $a_{\rm in} = 0.1$ au, and the SMBH has $a_{\rm out} = 500$ au (the initial eccentricities $e_{\rm in} = e_{\rm out} = 0.001$). The misalignment angle between $\hat{\boldsymbol{S}}_3$ and $\hat{\boldsymbol{L}}_{\rm out}$ is set to 30°, but with a random azimuthal phase angle. The values of $e_{\rm max}$ are calculated by DA secular equations, where the cyan dots are results (which can be obtained analytically; e.g., Liu et al. 2015) from "standard LK" and the purple dots include Effects I, II, and IV. In the bottom right panel, we also show the $e_{\rm max}$ obtained by integrating SA secular equations (light blue dots). The range of γ (as labeled) is given by Equation (10) evaluated at $I = 0$ and 180°. Effect III only influences the BH spin evolution, and thus does not play a role in the plot. We have also done calculations that do not include Effect IV, and found that the result is similar.

"adiabaticity parameters":

$$\mathcal{A} \equiv \left| \frac{\Omega_{\rm S_1L_{in}}}{\Omega_{\rm L_{in}L_{out}}} \right|, \mathcal{B} \equiv \frac{\Omega_{\rm S_1L_{in}}}{\Omega_{\rm S_1L_{out}}}. \quad (13)$$

We expect (i) when $\mathcal{A}, \mathcal{B} \ll 1$ ("nonadiabatic"), the spin axis $\hat{\boldsymbol{S}}_1$ cannot "keep up" with the rapidly changing $\hat{\boldsymbol{L}}_{\rm in}$, and thus effectively precesses around $\boldsymbol{L}_{\rm out}$, keeping $\theta_{\rm S_1L_{out}} \simeq$ constant (note that since $\Omega_{\rm S_1L_{out}} = \Omega_{\rm L_{in}L_{out}}$ is only a few times larger than $\Omega_{\rm L_{out}S_3}$—see Figure 1—$\theta_{\rm S_1L_{out}}$ is only approximately constant as $\hat{\boldsymbol{L}}_{\rm out}$ precesses around $\hat{\boldsymbol{S}}_3$); (ii) when $\mathcal{A}, \mathcal{B} \gg 1$ ("adiabatic"), $\hat{\boldsymbol{S}}_1$ closely "follows" $\hat{\boldsymbol{L}}_{\rm in}$, maintaining an approximately constant $\theta_{\rm sl}$. (iii) In the regime between (i) and (ii) ("trans-adiabatic"), the evolution of $\hat{\boldsymbol{S}}_1$ can be quite complicated and chaotic, because of its dependence on $e_{\rm in}$ during the LK cycles (see Storch et al. 2014; Storch & Lai 2015; Anderson et al. 2016, 2017; Liu & Lai 2017, 2018).

As the BHB orbit decays, the system may transition from "nonadiabatic" at large $a_{\rm in}$ to "adiabatic" at small $a_{\rm in}$, where the final spin–orbit misalignment angle $\theta_{\rm sl}^{\rm f}$ is "frozen." From Figure 1, we see that, because of the contribution of $\Omega_{\rm L_{in}L_{out}}^{\rm (GR)}$ to $\Omega_{\rm L_{in}L_{out}}$, the conditions $\mathcal{A}, \mathcal{B} \ll 1$ can be easily satisfied initially for systems with $m_3 \gtrsim 10^8 M_\odot$. As these systems experience LK-induced orbital decay, they must go through the "trans-adiabatic" regime and therefore may attain a wide range of $\theta_{\rm sl}^{\rm f}$ (see below).

(iv) *Effects IV*. Both $\hat{\boldsymbol{L}}_{\rm in}$ and $\hat{\boldsymbol{S}}_1$ (and $\hat{\boldsymbol{S}}_2$) experience Lens–Thirring precession around $\hat{\boldsymbol{S}}_3$ at the rate

$$\Omega_{\rm L_{in}S_3} = \Omega_{\rm S_1S_3} = \Omega_{\rm LT} = \frac{GS_3}{2c^2 a_{\rm out}^3 (1-e_{\rm out}^2)^{3/2}}. \quad (14)$$

Since $\Omega_{\rm L_{in}S_3}/\Omega_{\rm L_{in}L_{out}}^{\rm (GR)} = \Omega_{\rm S_1S_3}/\Omega_{\rm S_1L_{out}} \sim V_{\rm out}/c$ (where $V_{\rm out}$ is the orbital velocity of the outer binary), they can be neglected when $V_{\rm out}/c \ll 1$.

3. Binary BH Mergers Induced by SMBH

We now add gravitational radiation to our fiducial example (Figure 3 with $m_3 = 2.3 \times 10^9 M_\odot$). Since Effect IV is not important in this example, we perform two sets of calculations with and without Effects I-III, and evolve the system until the BHB enters the LIGO band (i.e., when the peak GW frequency reaches 10 Hz). The results are summarized in Figure 4.

In the "standard LK" mechansim (without Effects I-III; cyan circles in the top two panels of Figure 4), for systems with negligible octupole effects, the merger time can be well approximated by (e.g., Liu & Lai 2018)

$$T_{\rm m} \simeq T_{\rm m,0}(1-e_{\rm max}^2)^3, \quad (15)$$

where $T_{\rm m,0} \equiv (5c^5 a_{\rm in,0}^4)/(256 G^3 m_{12}^2 \mu_{\rm in})$ is the merger time due to GW emission for an isolated circular BHB (e.g., Peters 1964; $T_{\rm m,0} \simeq 10^9$ yr for the systems considered in Figure 4), and $e_{\rm max}$ is the maximum eccentricity achieved in the LK cycle (see Figure 3). When the GR effects associated with the SMBH are

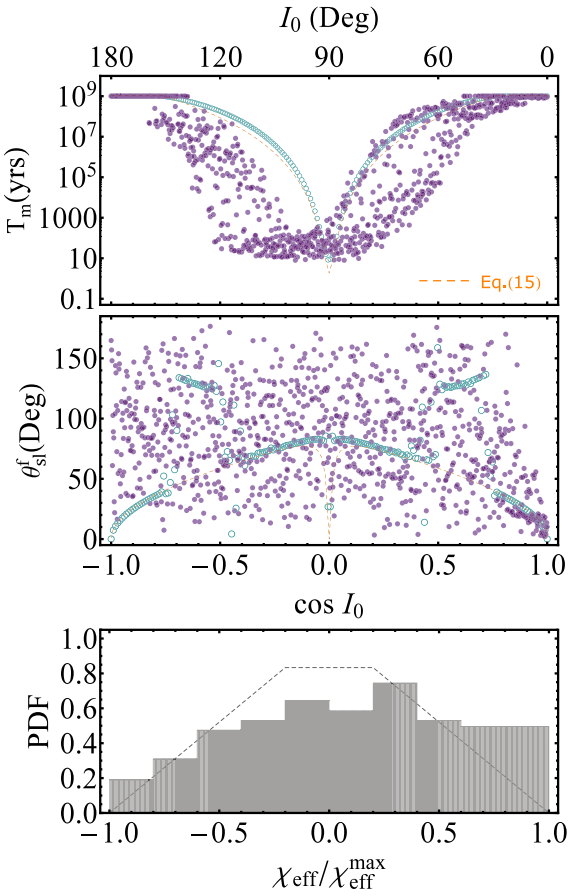

Figure 4. BHB merger time T_m (top panel) and final spin–orbit misalignment angle (middle panel) as a function of the initial inclination for the BHB–SMBH triple system. The purple dots are the results that include various new GR effects discussed in this Letter (Effects I-III), while the cyan circles do not. The bottom panel shows the distribution of the rescaled binary spin parameter χ_{eff} (with $\chi_{eff}^{max} = (m_1\chi_1 + m_2\chi_2)/m_{12}$ and assuming $\chi_1 = \chi_2$) for the "GR-enhanced" mergers (purple dots in the middle panel). The system parameters are the same as those in Figure 3 with $m_3 = 2.3 \times 10^9 M_\odot$. The dashed curve in the middle panel is given by the analytical expression derived for circular mergers in the presence of a tertiary Liu & Lai (2017), and the dashed line in the bottom panel shows the distribution for uncorrelated isotropic spins (Equation 81 in Liu & Lai 2018).

taken into account (purple dots), the range of inclinations for rapid mergers (shorter T_m) becomes much larger, a direct consequence of the widened LK eccentricity excitation window (see Figure 3). Note that in a dense nuclear cluster, the orbits of a BHB–SMBH triple system can be perturbed or disrupted by close flybys of other objects. If we introduce upper limits of the survival time for the triples, the "standard LK" would give the merger fraction of $f_{merger} \simeq 12\%, 20\%, 30\%$ for $T_m \lesssim 10^5, 10^6, 10^7$ yr, respectively, while including Effects I–III would increase the corresponding merger fraction to $f_{merger} \simeq 58\%, 63\%, 70\%$.

The middle panel of Figure 4 shows the distribution of θ_{sl}^f as a function of cos I_0.[6] In the "standard LK" (as studied in Liu & Lai 2017, 2018; Liu et al. 2019), the final spin axis shows a regular distribution when the octupole effects are negligible (as in the BHB–SMBH case studied here); for the systems that do not experience eccentricity excitation, an analytical expression for θ_{sl}^f can be obtained (Liu & Lai 2017; see the dashed line). However, when the GR effects associated with the SMBH are included, the final BH spin orientation is significantly "randomized." Given the wide distribution of θ_{sl}^f, we find the large spread in χ_{eff} in the bottom panel of Figure 4, where $\chi_{eff} = (m_1\boldsymbol{\chi}_1 + m_2\boldsymbol{\chi}_2) \cdot \hat{\boldsymbol{L}}_{in}/m_{12}$ (with $\boldsymbol{\chi}_{1,2} = c\boldsymbol{S}_{1,2}/(Gm_{1,2}^2)$) is the effective binary spin parameter that can be directly measured from GW observations. Note that the two spins in the merging binary BHs are strongly correlated (see also Liu et al. 2019; Figure 10); this is different for the scenarios involving strong scattering, which expectedly produce uncorrelated isotropic spins.

Due to the negligible octupole effect in BHB–SMBH systems, the "residual" eccentricities of merging BHBs (when they enter the 10 Hz LIGO band) are all below 0.1 in our simulations. This is in contrast to binary mergers induced by the stellar-mass tertiary studied in Liu et al. (2019).

4. Summary and Discussion

We have identified the impacts of several GR effects in BHB–SMBH triples that have been little explored. Effect I (Equations (4)–(6)) allows the BHB eccentricity to reach extremely high values even with modestly inclined or nearly coplanar outer orbits. Effect II (Equations (8) and (9)) modifies the eccentricity growth (when combined with Effect I) and BH spin evolution indirectly. Effect III (Equations (11) and (12)) only affects the spin evolution. The overall dynamics of the BHB and BH spin around an SMBH can be characterized by the dimensionless rates (Equations (10) and (13)). Effects I and II generally require very massive SMBH ($m_3 \gtrsim 10^8$–$10^9 M_\odot$) to be effective, while Effect III can be important for a wide range of SMBH masses (see Figure 1). Overall, these GR effects can significantly widen the LK-induced merger window and increase the merger fraction. They also produce a broad distribution of the final BH spin–orbit misalignment angles, leading to a wide range of the effective BHB spin parameter χ_{eff}.

Our proof-of-concept calculations have demonstrated the importance of the GR effects in BHB–SMBH systems. However, we have not thoroughly explored the relevant parameter space, nor considered various "environmental" effects associated with BHBs in nuclear cluster. We leave these to future works.

We thank Jean Teyssandier and Clifford Will for useful discussion and communication. This work is supported in part by the NSF grant AST-1715246 and NASA grant NNX14AP31G.

ORCID iDs

Bin Liu https://orcid.org/0000-0002-0643-8295
Dong Lai https://orcid.org/0000-0002-1934-6250

References

Abbott, B. P., Abbott, R., Abbott, T. D., et al. 2018a, LIGO Scientific and Virgo Collaboration, arXiv:1811.12907
Abbott, B. P., Abbott, R., Abbott, T. D., et al. 2018b, LIGO Scientific and Virgo Collaboration, arXiv:1811.12940
Anderson, K. R., Lai, D., & Storch, N. I. 2017, MNRAS, 467, 3066
Anderson, K. R., Storch, N. I., & Lai, D. 2016, MNRAS, 456, 3671
Antonini, F., & Perets, H. B. 2012, ApJ, 757, 27
Antonini, F., Rodriguez, C. L., Petrovich, C., & Fischer, C. L. 2018, MNRAS, 480, L58

[6] In a nuclear cluster, the initial binary BHs may have nontrivial spin orientations due to the complicated scattering processes. In order to have an intuitive understanding of the spin dynamics, here we assume that the BH spin axis is initially aligned with the orbital axis.

Antonini, F., Toonen, S., & Hamers, A. S. 2017, ApJ, 841, 77
Bahcall, J. N., & Wolf, R. A. 1976, ApJ, 209, 214
Banerjee, S., Baumgardt, H., & Kroupa, P. 2010, MNRAS, 402, 371
Barker, B. M., & O'Connell, R. F. 1975, PhRvD, 12, 329
Blaes, O., Lee, M. H., & Socrates, A. 2002, ApJ, 578, 775
Downing, J. M. B., Benacquista, M. J., Giersz, M., & Spurzem, R. 2010, MNRAS, 407, 1946
Fabrycky, D., & Tremaine, S. 2007, ApJ, 669, 1298
Fang, Y., & Huang, Q.-G. 2019, PhRvD, 99, 103005
Frangione, G., Ginsburg, I., & Loeb, A. 2019, arXiv:1907.08008
Gondán, L., Kocsis, B., Raffai, P., et al. 2018, ApJ, 860, 5
Hamers, A. S. 2018, MNRAS, 478, 620
Hamers, A. S., Bar-Or, B., Petrovich, C., et al. 2018, ApJ, 865, 2
Hamers, A. S., & Lai, D. 2017, MNRAS, 470, 1657
Hoang, B.-M., Naoz, S., Kocsis, B., Rasio, F. A., & Dosopoulou, F. 2018, ApJ, 856, 140
Kiseleva, L. G., Aarseth, S. J., Eggleton, P. P., & de La Fuente Marcos, R. 1996, in ASP Conf. Ser. 90, The Origins, Evolution, and Destinies of Binary Stars in Clusters, ed. E. F. Milone & J.-C. Mermilliod (San Francisco, CA: ASP), 433
Leigh, N. W. C., Geller, A. M., McKernan, B., et al. 2018, MNRAS, 474, 5672
Liu, B., & Lai, D. 2017, ApJL, 846, L11
Liu, B., & Lai, D. 2018, ApJ, 863, 68
Liu, B., & Lai, D. 2019, MNRAS, 483, 4060
Liu, B., Lai, D., & Wang, Y.-H. 2019, ApJ, 881, 41
Liu, B., Muñoz, D. J., & Lai, D. 2015, MNRAS, 447, 747
Luo, L., Katz, B., & Dong, S. 2016, MNRAS, 458, 3060
Miller, M. C., & Hamilton, D. P. 2002, ApJ, 576, 894
Miller, M. C., & Lauburg, V. M. 2009, ApJ, 692, 917
O'Leary, R. M., Kocsis, B., & Loeb, A. 2009, MNRAS, 395, 2127
O'Leary, R. M., Rasio, F. A., Fregeau, J. M., Ivanova, N., & O'Shaughnessy, R. 2006, ApJ, 637, 937
Peters, P. C. 1964, PhRv, 136, B1224
Petrovich, C. 2015, ApJ, 799, 27
Petrovich, C., & Antonini, F. 2017, ApJ, 846, 146
Portegies, Z. S. F., & McMillan, S. L. W. 2000, ApJL, 528, L17
Randall, L., & Xianyu, Z.-Z. 2018, ApJ, 853, 93
Rodriguez, C. L., Amaro-Seoane, P., Chatterjee, S., & Rasio, F. A. 2018, PhRvL, 120, 151101
Rodriguez, C. L., & Antonini, F. 2018, ApJ, 863, 7
Samsing, J., & D'Orazio, D. J. 2018, MNRAS, 481, 5445
Samsing, J., D'Orazio, D. J., Askar, A., & Giersz, M. 2018, arXiv:1802.08654
Samsing, J., & Ramirez-Ruiz, E. 2017, ApJL, 840, L14
Silsbee, K., & Tremaine, S. 2017, ApJ, 836, 39
Storch, N. I., Anderson, K. R., & Lai, D. 2014, Sci, 345, 1317
Storch, N. I., & Lai, D. 2015, MNRAS, 448, 1821
VanLandingham, J. H., Miller, M. C., Hamilton, D. P., & Richardson, D. C. 2016, ApJ, 828, 77
Venumadhav, T., Zackay, B., Roulet, J., Dai, L., & Zaldarriaga, M. 2019, arXiv:1904.07214
Wen, L. 2003, ApJ, 598, 419
Will, C. M. 2014, PhRvD, 89, 044043
Will, C. M. 2018, PhRvL, 120, 191101
Zackay, B., Venumadhav, T., Dai, L., Roulet, J., & Zaldarriaga, M. 2019, PhRvD, 100, 023007
Ziosi, B. M., Mapelli, M., Branchesi, M., et al. 2014, MNRAS, 441, 3703